

B_c^\pm - ^{12}C states and detailed study of momentum space method for Υ - and η_b -nucleus bound states

G. N. Zeminiani,^{1,*} J.J. Cobos-Martínez,^{2,†} and K. Tsushima^{1,‡}

¹*Laboratório de Física Teórica e Computacional (LFTC),*

Programa de Pósgraduação em Astrofísica e Física Computacional,

Universidade Cidade de São Paulo (UNICID), 01506-000, São Paulo, SP, Brazil

²*Departamento de Física, Universidad de Sonora, Boulevard Luis Encinas J. y Rosales,*

Colonia Centro, Hermosillo, Sonora 83000, México

We perform a detailed study of the Υ -, η_b -, and B_c -nucleus systems in momentum space to calculate the bound-state energies and the corresponding coordinate-space radial wave functions. The attractive strong potentials for the meson-nucleus systems are calculated from the Lorentz scalar mass modifications of these mesons in nuclear matter in the local density approximation in the nucleus. The downward shift of the meson masses may be regarded as a signature of partial restoration of chiral symmetry in a nuclear medium applied in the present study in an empirical sense, because the origin of the negative mass shift in this study is not directly related to the chiral symmetry mechanism. Furthermore, as an initial and realistic study, the B_c^\pm - ^{12}C bound states are studied for the first time, with the effects of self-consistently calculated Coulomb potentials in ^{12}C (when the B_c^\pm mesons are absent).

I. INTRODUCTION

Studies of hadron properties under extreme conditions indicate that the Lorentz scalar effective masses of mesons are expected to decrease in a nuclear medium, as a consequence of partial restoration of chiral symmetry [1–4]. This negative effective mass shift (Lorentz scalar) of the meson can be regarded as an attractive Lorentz scalar potential, and when the sum of the Lorentz scalar and the Lorentz vector potentials (total potential in a nonrelativistic sense) is sufficiently attractive, the mesons can be bound to atomic nuclei. In 1985, Friedman and Soff discussed deeply bound pionic states in heavy atomic nuclei [5], which were first observed in 1996 in the $^{208}\text{Pb}(d, ^3\text{He})$ reaction [6]. That led to predictions of other possible meson-nucleus bound states [7–9]. In the case of heavy quarkonia (no vector potentials arise in the lowest order), charmonium-nucleus systems were proposed in 1989 [10], which led to various subsequent studies [1, 2, 11–30] and lattice QCD calculations [31–33] on these states. Recent lattice results show also a possibility of ϕ -nucleon (N) bound states [34], although ϕ is not the heavy quarkonium. Furthermore, by the developed Faddeev three-body approach using the lattice extracted ϕ - N potential, a possible ϕ - NN bound state is predicted [35]. We have studied further the bottomonium-nucleus systems [1, 30] and predicted that the Υ and η_b mesons can form strong nuclear bound states with various nuclei [36–39], provided that they are produced inside a nucleus with very low relative momenta to the nucleus.

The Okubo-Zweig-Iizuka rule dictates the suppression of the light hadron exchange in the heavy quarkonium-nucleus interaction, and then the interaction must occur primarily by multigluon exchange, namely, a QCD van der Waals type of interaction [26]. Looking at different possibilities, we consider an alternative (effective) mechanism for the quarkonium-nucleus interaction. We estimated the charmonia (J/Ψ and η_c) and bottomonia (Υ and η_b) mass modifications (Lorentz scalar) by the enhanced in-medium self-energies via the excitations of intermediate-state hadrons with light quarks [30].

The focus of the present study is first the bottomonia, for which the self-energies were calculated including only the minimal loop contributions for the Υ and η_b mesons, namely, the BB loop for the Υ , and the BB^* loop for the η_b [36]. The calculations are performed neglecting any possible imaginary part of the self-energies. Second, we study the B_c^\pm -nucleus bound states for the first time, with and without the Coulomb force.

*Electronic address: guilherme.zeminiani@gmail.com

†Electronic address: jesus.cobos@unison.mx

‡Electronic address: kazuo.tsushima@gmail.com, kazuo.tsushima@cruzeirodosul.edu.br

To obtain the bound-state energies and the corresponding bound meson state wave functions of the meson-nucleus systems in the coordinate space, we solve the Klein-Gordon equation in momentum space, where for the Υ case, the Proca equation is approximated and reduced to the Klein-Gordon equation assuming the longitudinal and transverse modes are nearly equal with low momentum. It is very convenient to deal with the kinetic term in the Klein-Gordon equation in momentum space, and the search for the bound-state energies is also much simpler than performing in coordinate space. This can be done by solving the differential wave equation as an eigenvalue equation, and using a method for finding selected eigenvalues and eigenfunctions (eigen vectors). This makes it easy to extend the calculation for complex Hamiltonians, e.g., when including the meson widths and/or imaginary potentials. In coordinate space, dealing with complex eigenvalues is tricky, as it involves searching for a convergence point in the real and imaginary parts in energy plane, as well as the real and imaginary parts of the coordinate-space wave functions.

The bound-state energies calculated for Υ - ^{12}C , Υ - ^4He , η_b - ^{12}C and η_b - ^4He systems reported in Ref. [39], are calculated again here and compared with the present results, for which we present in this study for the first time the wave functions in coordinate space associated with each energy level of the bound state. In this article we also report the first results of the B_c -nucleus bound states, for B_c - ^4He and B_c - ^{12}C with no Coulomb interaction, followed by a realistic study of B_c^\pm - ^{12}C including the Coulomb potentials, where the Coulomb potentials are calculated self-consistently in the ^{12}C nucleus when the B_c^\pm mesons are absent, within the quark-meson coupling (QMC) model treatment for finite nuclei [40–46].

This article is organized as follows. In Sec. II we discuss the downward shift masses of the Υ , η_b and B_c mesons in nuclear matter. In Sec. III we relate the mass shift with the attractive meson-nucleus potentials and discuss the method used to solve the Klein-Gordon equation in momentum space. The numerical procedure of the calculation is explained in Sec. IV, and the results are presented in Sec. V. An initial study of the B_c - ^4He (no Coulomb potential) and B_c^\pm - ^{12}C bound states (with and without the Coulomb potentials) is made in Sec. VI. The summary and conclusions are given in Sec. VII.

II. MESON MASS SHIFT IN NUCLEAR MATTER

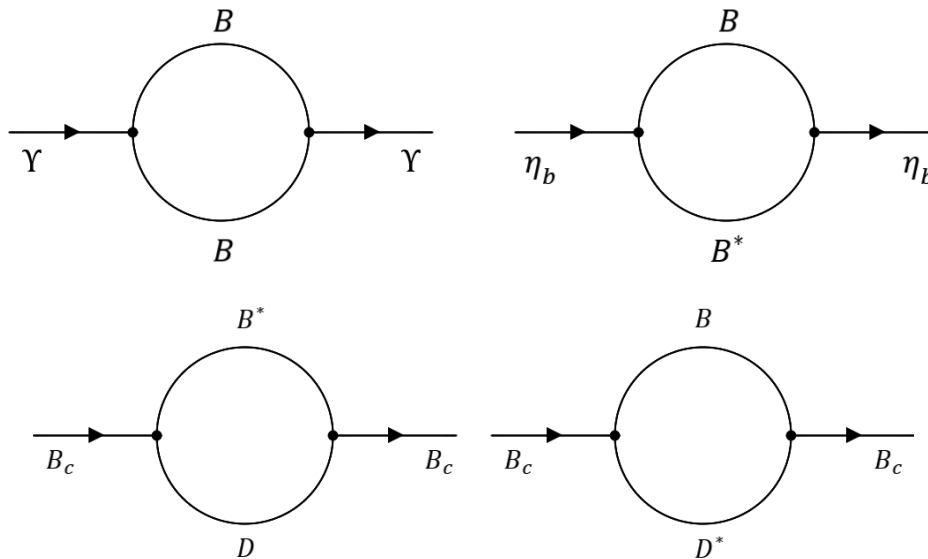


FIG. 1: Diagrammatic representation of the lowest order one-loop contributions to the Υ (top left), η_b (top right) and B_c (bottom) self-energies.

The mass shift of the Υ , η_b , and B_c mesons originates from the medium modifications of the intermediate state meson loop contributions to their self-energies, represented in Fig. 1. The self-energies are calculated based on the following effective Lagrangian (densities) for each vertex derived from a flavor SU(5) symmetric effective Lagrangian (density) [36]

$$\begin{aligned}
\mathcal{L}_{\Upsilon BB} &= ig_{\Upsilon BB} \Upsilon^\mu [\bar{B} \partial_\mu B - (\partial_\mu \bar{B}) B], \\
\mathcal{L}_{\eta_b BB^*} &= ig_{\eta_b BB^*} \{ (\partial^\mu \eta_b) (\bar{B}^*{}_\mu B - \bar{B} B^*_\mu) - \eta_b [\bar{B}^*{}_\mu (\partial^\mu B) - (\partial^\mu \bar{B}) B^*_\mu] \}, \\
\mathcal{L}_{B_c B^* D} &= ig_{B_c B^* D} [(\partial_\mu B_c^-) D - B_c^- (\partial_\mu D)] B^{*\mu} + H.c., \\
\mathcal{L}_{B_c B D^*} &= ig_{B_c B D^*} [(\partial_\mu B_c^+) \bar{B} - B_c^+ (\partial_\mu \bar{B})] \bar{D}^{*\mu} + H.c.,
\end{aligned} \tag{1}$$

where the following conventions are used

$$\begin{aligned}
B &= \begin{pmatrix} B^+ \\ B^0 \end{pmatrix}, & \bar{B} &= \begin{pmatrix} B^- & \bar{B}^0 \end{pmatrix}, & B^* &= \begin{pmatrix} B^{*+} \\ B^{*0} \end{pmatrix}, & \bar{B}^* &= \begin{pmatrix} B^{*-} & \bar{B}^{*0} \end{pmatrix}, \\
\bar{D} &= \begin{pmatrix} \bar{D}^0 \\ D^- \end{pmatrix}, & D &= \begin{pmatrix} D^0 & D^+ \end{pmatrix}, & \bar{D}^* &= \begin{pmatrix} \bar{D}^{*0} \\ D^{*-} \end{pmatrix}, & D^* &= \begin{pmatrix} D^{*0} & D^{*+} \end{pmatrix}.
\end{aligned}$$

The SU(5) symmetric universal coupling g is fixed by $g_{\Upsilon BB} = \frac{5g}{4\sqrt{10}} \approx 13.2$ by the Υ decay data $\Gamma(\Upsilon \rightarrow e^+ e^-)$ with the vector meson dominance (VMD) model [36], and thus we get

$$g_{\eta_b BB^*} = g_{\Upsilon BB} \approx 13.2, \quad g_{B_c B^* D} = g_{B_c B D^*} = \frac{2}{\sqrt{5}} g_{\Upsilon BB} = \frac{g}{2\sqrt{2}} \approx 11.9. \tag{2}$$

The in-medium Lorentz scalar potential, or the mass shift value, for the heavy mesons $h(=\Upsilon, \eta_b, B_c)$ is given by the difference of the in-medium m_h^* and the free space m_h masses

$$V = m_h^* - m_h, \tag{3}$$

with the free-space physical mass being self-consistently reproduced by

$$m_h^2 = (m_h^0)^2 - |\Sigma_h(k^2 = m_h^2)|, \tag{4}$$

where m_h^0 is the bare mass and Σ_h is the total self-energy. The in-medium mass m_h^* is calculated likewise, with the same bare mass value m_h^0 determined in free space, and the in-medium masses of the B , B^* , D , and D^* mesons are calculated using the QMC model [40, 41, 44]. Neglecting any possible effects of the widths, the self-energies in medium are given below for each meson

$$\begin{aligned}
\Sigma_\Upsilon^{BB}(m_\Upsilon^*) &= \left(-\frac{g_{\Upsilon BB}^2}{3\pi^2}\right) \int_0^\infty d|\mathbf{k}| |\mathbf{k}|^2 I_\Upsilon^{BB}(|\mathbf{k}|) F_{\Upsilon BB}(\mathbf{k}^2) \\
\Sigma_{\eta_b}^{BB^*}(m_{\eta_b}^*) &= \frac{8g_{\eta_b BB^*}^2}{\pi^2} \int_0^\infty d|\mathbf{k}| |\mathbf{k}|^2 I_{\eta_b}^{BB^*}(|\mathbf{k}|) F_{\eta_b BB^*}(\mathbf{k}^2) \\
\Sigma_{B_c}^{B^* D}(m_{B_c}^*) &= \frac{-4g_{B_c B^* D}^2}{\pi^2} \int d|\mathbf{k}| |\mathbf{k}|^2 I_{B_c}^{B^* D}(|\mathbf{k}|) F_{B_c B^* D}(\mathbf{k}^2),
\end{aligned} \tag{5}$$

where

$$\begin{aligned}
I_{\Upsilon}^{BB}(|\mathbf{k}|) &= \frac{1}{\omega_B^*} \left(\frac{|\mathbf{k}|^2}{\omega_B^{*2} - m_{\Upsilon}^{*2}/4} \right), \\
I_{\eta_b}^{BB^*}(|\mathbf{k}|) &= \frac{m_{\eta_b}^{*2}(-1 + (k^0)^2/m_{B^*}^{*2})}{(k^0 + \omega_{B^*}^*)(k^0 - \omega_{B^*}^*)(k^0 - m_{\eta_b}^* - \omega_B^*)} \Big|_{k^0=m_{\eta_b}^*-\omega_B^*} \\
&\quad + \frac{m_{\eta_b}^{*2}(-1 + (k^0)^2/m_{B^*}^{*2})}{(k^0 - \omega_{B^*}^*)(k^0 - m_{\eta_b}^* + \omega_B^*)(k^0 - m_{\eta_b}^* - \omega_B^*)} \Big|_{k^0=-\omega_{B^*}^*}, \\
I_{B_c}^{B^*D}(|\mathbf{k}|) &= \frac{m_{B_c}^{*2}(-1 + (k^0)^2/m_{B^*}^{*2})}{(k^0 - \omega_{B^*}^*)(k^0 - m_{B_c}^* + \omega_D^*)(k^0 - m_{B_c}^* - \omega_D^*)} \Big|_{k^0=-\omega_{B^*}^*} \\
&\quad + \frac{m_{B_c}^{*2}(-1 + (k^0)^2/m_{B^*}^{*2})}{(k^0 + \omega_{B^*}^*)(k^0 - \omega_{B^*}^*)(k^0 - m_{B_c}^* - \omega_D^*)} \Big|_{k^0=m_{B_c}^*-\omega_D^*}, \tag{6}
\end{aligned}$$

and $\omega_{B^*,D^*}^* = (\mathbf{k}^2 + m_{B^*,D^*}^{*2})^{1/2}$. [A similar calculation has been performed for $\Sigma_{B_c}^{B^*D^*}(m_{B_c}^*)$, and will be reported in the future.] To regularize the divergence in the loop integral we introduce into the integrand a regularizing function given by the product of the vertex form factors. We use the following form factors for the vertex in-medium as (now the in-medium meson masses enter, instead of free meson masses): $F_{B_c B^* D}(\mathbf{k}^2) = u_{B_c B^*}(\mathbf{k}^2) u_{B_c D}(\mathbf{k}^2)$, where $u_{B_c B^*} = \left(\frac{\Lambda_{B^*}^2 + m_{B_c}^{*2}}{\Lambda_{B^*}^2 + 4\omega_{B^*}^{*2}(\mathbf{k}^2)} \right)^2$ and $u_{B_c D} = \left(\frac{\Lambda_D^2 + m_{B_c}^{*2}}{\Lambda_D^2 + 4\omega_D^2(\mathbf{k}^2)} \right)^2$ with Λ_{B^*} and Λ_D being the cutoff masses associated with the B^* and D mesons, respectively. Similar form factors are used for the other vertices. We use a common value for the cutoff parameter $\Lambda \equiv \Lambda_{B^*,D^*}$, ranging $\Lambda = 2000, 3000, 4000, 5000$, and 6000 MeV and see the ambiguities by the values on the final results.

Solving Eq. (4) with the self-energy calculated with the medium-modified intermediate-state meson masses, we estimate the nuclear density dependent mass shift, presented in Fig. 2 as a function of the nuclear matter density (ρ_B/ρ_0) for the different values of the cutoff mass Λ .

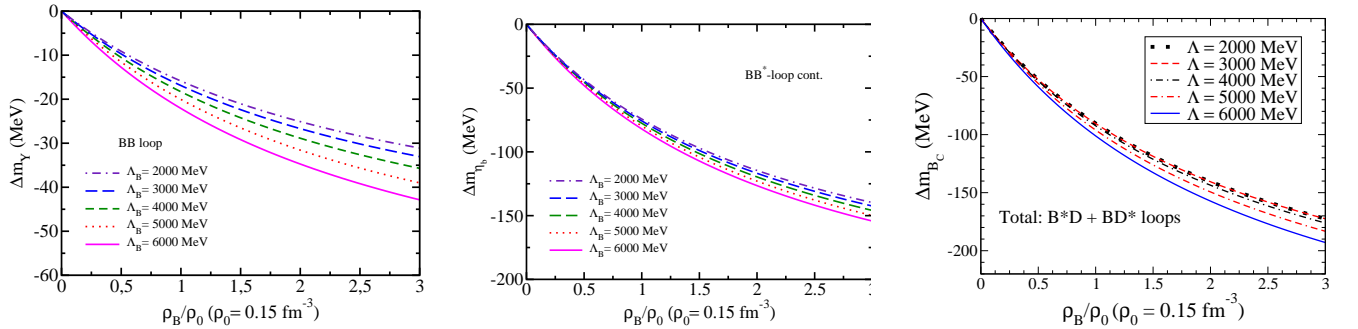


FIG. 2: In-medium mass shift of Υ (left), η_b (center) and B_c (right) mesons versus baryon density (ρ_B/ρ_0) for five different values of the cutoff mass Λ .

III. NUCLEAR BOUND STATES

First, we study the bottomonium-nucleus bound states. The coordinate-space nuclear potentials for the systems Υ - ^4He , Υ - ^{12}C , η_b - ^4He and η_b - ^{12}C are calculated using a local density approximation. For a bottomonium $h(=\Upsilon, \eta_b)$ and a nucleus A , the potential is given by the equation

$$V_{h-A}(r = |\vec{r}|) = \Delta m_h(\rho_B^A(r)) \equiv m_h^*(r) - m_h, \tag{7}$$

where r is the distance from the center of the nucleus, Δm_h is the value of the meson mass shift (Lorentz scalar), m_h^* being the in-medium effective Υ or η_b mass in nuclear matter, and $\rho_B^A(r)$ is the nuclear density distribution in

the nucleus A . For the ^{12}C nucleus, it was calculated by the QMC model [44], and for the ^4He nucleus we use the parameterized nuclear density from Ref. [47]. The potentials are shown in Fig. 3.

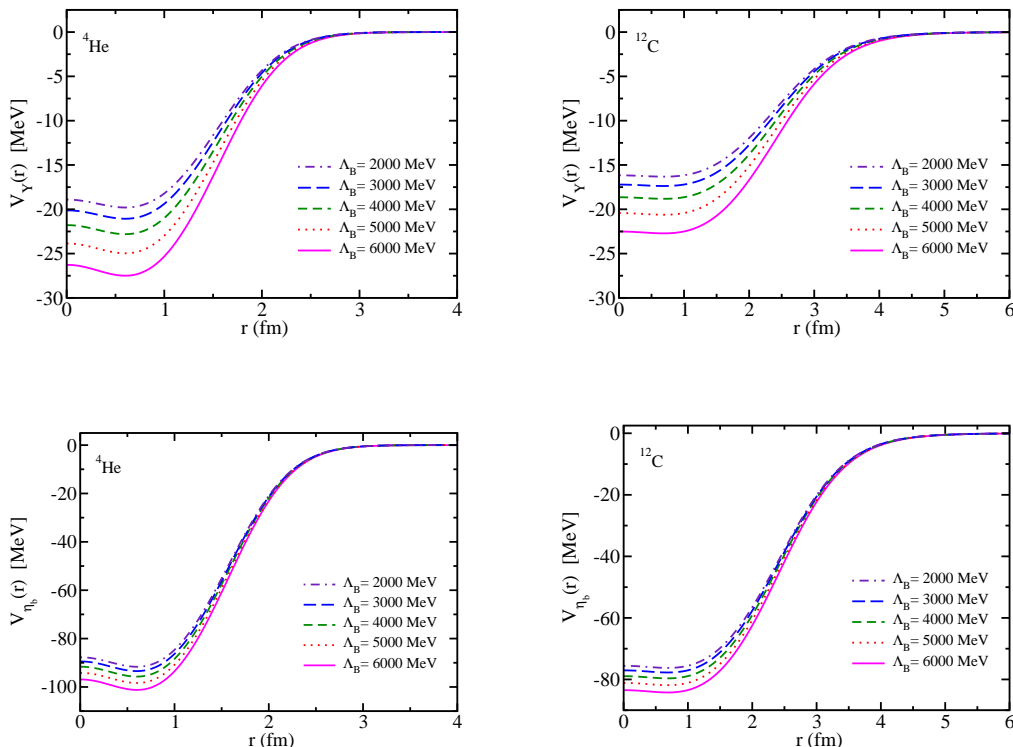


FIG. 3: Nuclear (Lorentz scalar) potentials for the Υ - ^4He (top-left), Υ - ^{12}C (top-right), η_b - ^4He (bottom-left) and η_b - ^{12}C (bottom-right) systems for different values of the cutoff parameter Λ .

The meson-nucleus bound states are studied first in momentum space by solving the Klein-Gordon (K.G.) equation. While the K.G. equation is solved for the pseudoscalar η_b meson, we also solve the K.G. equation for the spin-1 Υ meson. This is based on the approximation (assuming the case) that the Υ -nucleus relative momentum is nearly zero. In this situation, the transverse and longitudinal components in the Proca equation are expected to be very similar, which allows us to reduce it to solving a single-component K.G. equation, as practiced in Refs. [37–39]. The η_b - and Υ -nuclear potentials were previously calculated in coordinate space in Ref. [39], in which they were transformed into the momentum-space by one particular method for that study (“Woods-Saxon Fourier transform” method to be explained later). For the purpose of the present study, we will transform the coordinate-space potentials using another method. A comparison of the results obtained by the different methods is presented in the Appendix A.

We solve the K.G. equation in momentum space of the form

$$\left[\vec{P}^2 + (m + V_N)^2 \right] \psi = \varepsilon^2 \psi, \quad (8)$$

where \vec{P} is the “relative momentum” of the meson and the nucleus, ψ is the momentum-space wave function of the system, m is the reduced mass of the meson-nucleus system ($m = m_h m_A / (m_h + m_A)$, m_h is the meson mass and m_A the nucleus mass) and V_N is the Lorentz scalar nuclear potential in momentum space, where $V_N(r) \equiv V_{h-A}(r)$. The K.G. equation will be solved for each value of the angular momentum ℓ of the meson-nucleus system to calculate the bound-state energies and to get the momentum-space eigen wave function corresponding to each bound-state energy level of the system.

The partial wave solutions for the bound-state energies and the corresponding wave functions of the K.G equation require the decomposition of the meson-nucleus potential into a given angular momentum ℓ wave. Generally, a straightforward way to obtain the ℓ -wave decomposition of the meson-nucleus potential $V_N(r)$ is to apply the double

spherical Bessel transform,

$$V_{N\ell}(P, P') = \frac{2}{\pi} \int_0^\infty dr r^2 j_\ell(Pr) j_\ell(P'r) V_N(r), \quad (9)$$

where j_ℓ ($\ell = 0, 1, 2, \dots$) are the spherical Bessel functions. (The reason why the potential has two arguments P and P' will become clearer in the next section.)

Since this transformation contains spherical Bessel functions, the oscillatory behavior of these functions must be tamed properly in order to construct the wave function in momentum space, as well as when the momentum-space wave function is transformed to the coordinate space for each partial wave ℓ solution. This is achieved by tuning the r and P grids to construct suitable discrete sets. More explanations on this will be given in a later section.

IV. NUMERICAL PROCEDURE

The partial wave expansion of Eq. (8) is given by

$$\begin{aligned} \varepsilon_{n\ell}^2 \psi_{n\ell}(P) &= (P^2 + m^2) \psi_{n\ell}(P) + 2m \int_0^\infty dP' P'^2 V_{N\ell}(P, P') \psi_{n\ell}(P') \\ &+ \int_0^\infty dP' P'^2 \left[\int_0^\infty dP'' P''^2 V_{N\ell}(P, P'') V_{N\ell}(P'', P') \right] \psi_{n\ell}(P'). \end{aligned} \quad (10)$$

The discretized Eq. (10) can be written in matrix form as

$$\sum_{j=1}^{NP} \hat{H}_{ij} \hat{\psi}_j = \varepsilon_{n\ell}^2 \hat{\psi}_i, \quad (11)$$

where $\hat{\psi}_i = \psi_{n\ell}(P_i)$. The matrix elements of the Hamiltonian are

$$\hat{H}_{ij} = (P_i^2 + m^2) \delta_{ij} + 2m P_j^2 w_j V_{N\ell}(P_i, P_j) + \left(\sum_{k=1}^{NP} P_k^2 w_k V_{N\ell}(P_i, P_k) V_{N\ell}(P_k, P_j) \right) P_j^2 w_j, \quad (12)$$

where NP is the number of points for the momentum grid, and P_i and w_j are respectively the i th momentum point and j th weight.

Equation (11) can be solved as an eigenvalue equation using iterative methods, such as the inverse iteration [48]. It is a method for finding selected eigenvalues and eigenfunctions, that has the advantage of only requiring the inversion of an $NP \times NP$ matrix. The equation to be solved is of the type

$$H |\psi_n\rangle = \varepsilon_n |\psi_n\rangle. \quad (13)$$

We begin with some guess value τ_n , and constructing the operator

$$B_n = (H - \tau_n)^{-1}, \quad (14)$$

that contains the Hamiltonian of Eq. (13). Next, we construct a state $|\chi_n^0\rangle$ that can be expressed using the complete set of eigenfunctions $|\psi_n\rangle$

$$|\chi_n^0\rangle = \sum_{n'} C_{n'} |\psi_{n'}\rangle, \quad (15)$$

which is multiplied N times by the operator B_n , resulting in

$$|\chi_n^N\rangle = (B_n)^N |\chi_n^0\rangle = \sum_{n'} C_{n'} (\varepsilon_{n'} - \tau_n)^{-N} |\psi_{n'}\rangle. \quad (16)$$

For nondegenerate eigenstates and for a proper guess τ_n , $n' = n$ will rapidly take over the sum. Then, for a large enough N

$$\begin{aligned} |\chi_n^N\rangle &\approx C_n (\varepsilon_n - \tau_n)^{-N} |\psi_n\rangle, \\ |\chi_n^{N+1}\rangle &\approx (\varepsilon_n - \tau_n)^{-1} |\chi_n^N\rangle, \end{aligned} \quad (17)$$

which can be written in a momentum-space calculation as

$$\begin{aligned}\chi_n^N(P) &\approx C_n(\varepsilon_n - \tau_n)^{-N}\psi_n(P), \\ \chi_n^{N+1}(P) &\approx (\varepsilon_n - \tau_n)^{-1}\chi_n^N(P).\end{aligned}\quad (18)$$

To facilitate the iterative numerical calculation, $\chi_n^N(P)$ is divided by its element with maximum modulus, $\tilde{\chi}_n^N(P) = \chi_n^N(P)/|\chi_n^N(P)|_{\max}$, and $\chi_n^{N+1}(P)$ is redefined as

$$\chi_n^{N+1}(P) \equiv B_n \tilde{\chi}_n^N(P), \quad (19)$$

and for sufficiently large N ,

$$|\chi_n^N(P)|_{\max} = \frac{1}{\varepsilon_n - \tau_n}, \quad \tilde{\chi}_n^N(P) = \frac{\psi_n(P)}{|\psi_n(P)|_{\max}}. \quad (20)$$

The eigenvalue is then given by

$$\varepsilon_n = \tau_n + \frac{1}{|\chi_n^N(P)|_{\max}}. \quad (21)$$

In the same way, the eigenvector $\psi_n(P)$ is determined by Eq. (20). The obtained eigenvalue and eigenvector are the system's eigenenergy and momentum-space wave function, respectively, for each n and ℓ .

A. Selection of gridpoints

There are two sets of gridpoints used to perform the numerical calculations: The r and the P gridpoints. These points must be properly chosen to be able to perform correctly the Gaussian integrations in Eqs. (9) and (12). In particular, the choice of grid in momentum space is not trivial compared to that in coordinate space, and one needs some care.

For the double spherical Bessel transform, one is recommended to properly limit the maximum number of points, so that the spherical Bessel functions, depending on both r and P grids, do not cause many oscillations. This is necessary to obtain the stable and nonexcessively oscillating wave functions (more explanations later). Furthermore, the r grid should contain the proper and sufficient points in the region where the potential is relevant. For example, the potentials presented in Fig. 3 are relevant in the region from $r = 0$ fm up to $r = 2$ or 3 fm. This means that most of the r gridpoints should be in this region close to the center of the nucleus, leaving fewer points to the region outside of this. A good choice for the momentum gridpoints in this integration is found to be $P \approx 1/r$.

When constructing the Hamiltonian, however, the P distribution of points is not necessarily the same as when performing the spherical Bessel transform. This is because of the kinetic term in the Hamiltonian. When transforming the potential to the momentum space, one should consider primarily the points where the potential is relevant, whereas in constructing the Hamiltonian of the system, Eq. (12), the points in the momentum corresponding to the regions in coordinate space further away from the center of nucleus must also be included. We use the points $P_i = \tan[\frac{1}{4}\pi(1 + x_i)]$ following Ref. [49], where x_i are the Gaussian points defined in the region $x_i = [-1, 1]$.

V. RESULTS

After solving numerically Eq. (11), we can obtain the bound-state energies of the meson-nucleus system, that are given by $E_{n\ell} = \varepsilon_{n\ell} - m$. The results are presented in Table I for the central value of the cutoff parameter $\Lambda = 4000$ MeV. A comparison for different values of Λ is presented in the Appendix A so that one can have ideas on the Λ -value dependence. We have obtained the energy levels by varying the eigenvalue initial guess, τ_n , for fixed ℓ . To get each eigenvalue, a different initial guess value is chosen, and this is repeated until all the desired energy levels are obtained. Each converged eigenvalue is then confirmed by analysing the number of nodes in the corresponding coordinate-space wave function. (Detailed explanations are given in next subsection.)

A. Coordinate-space wave functions

From the eigenvectors that come out as solutions of Eq. (11), we can use a (single) spherical Bessel transform to obtain the coordinate-space wave functions of the corresponding energy levels of the system:

$$\psi_{n\ell}(r = |\vec{r}|) = \frac{1}{2\pi} \int_0^\infty dP P^2 j_\ell(Pr) \psi_{n\ell}(P), \quad (22)$$

TABLE I: ${}^4_{\Upsilon}\text{He}$, ${}^{12}_{\Upsilon}\text{C}$, ${}^4_{\eta_b}\text{He}$ and ${}^{12}_{\eta_b}\text{C}$ bound state energies for the central value of the cutoff parameter $\Lambda = 4000$ MeV.

		$E_{n\ell}$ (MeV)
		$\Lambda = 4000$ MeV
${}^4_{\Upsilon}\text{He}$	1s	-6.25
${}^{12}_{\Upsilon}\text{C}$	1s	-15.26
	1p	-9.57
${}^4_{\eta_b}\text{He}$	1s	-71.59
	1p	-41.50
	1d	-39.56
	2s	-30.09
${}^{12}_{\eta_b}\text{C}$	1s	-66.93
	1p	-55.13
	1d	-48.50
	2s	-36.30
	1f	-28.09
	2p	-20.67

where the normalization is performed in $\psi_{n\ell}(P)$ according to the convention (recall that the wave functions are real in the present study),

$$\int \psi_{n\ell}(P)\psi_{n\ell}(P)P^2dP = 1. \quad (23)$$

As commented already, this procedure enables us to confirm that the obtained eigen energies are indeed corresponding to the correct eigen wave functions.

The gridpoints used in this integration may better be the same as those used to obtain the partial wave decomposition of the nuclear potential, namely the same as those when performing the double spherical Bessel transform. Otherwise the resultant wave function would be often unstable, with exceeding oscillations. We have observed that, the more the grid points differ from the corresponding points used for the partial wave decomposition, the more oscillations in the wave function are. For this reason, when one performs the spherical Bessel transform of the potential, one needs to chose properly the gridpoints that result in a smooth wave function.

The results for the Υ - ${}^4\text{He}$, Υ - ${}^{12}\text{C}$, η_b - ${}^4\text{He}$, and η_b - ${}^{12}\text{C}$ wave functions, for the central value of the cutoff parameter $\Lambda = 4000$ MeV are presented in Fig. 4.

VI. INITIAL STUDY OF THE B_c^\pm - ${}^4\text{He}$ AND B_c^\pm - ${}^{12}\text{C}$ BOUND STATES WITH AND WITHOUT THE COULOMB POTENTIALS

We now proceed to an initial study of the B_c^\pm - ${}^4\text{He}$ (without the Coulomb potentials) and B_c^\pm - ${}^{12}\text{C}$ bound states (with and without the Coulomb potentials). The mass shift of B_c meson in symmetric nuclear matter was calculated in Ref. [50], and we obtain the B_c -nucleus strong potential using a local density approximation. For a realistic calculation, the Coulomb potentials should enter for B_c^\pm -nucleus potentials, but they are absent in the Υ and η_b cases. First, we include only the strong interaction part of the B_c^\pm - ${}^4\text{He}$ and B_c^\pm - ${}^{12}\text{C}$ potentials, without the Coulomb potentials. Second, including the Coulomb potentials, we study the B_c^\pm - ${}^{12}\text{C}$ bound states, and focus on the role of the Coulomb potentials. This is because the ${}^{12}\text{C}$ nucleus is constructed self-consistently by the QMC model (relativistic, quark-based nuclear shell model), but this is not done for the ${}^4\text{He}$ nucleus.

The strong interaction potentials for B_c are presented in Fig. 5. These are calculated in the same manner as those for the Υ and η_b cases. We solve the K.G. equation and obtain the bound-state energies for the central value of the cutoff parameter $\Lambda = 4000$ MeV, which we present in Table II. The corresponding wave functions are shown in Fig. 6.

We now study the more realistic case for the B_c^\pm - ${}^{12}\text{C}$, where we include the Coulomb interaction. Including the Coulomb potential V_c in Eq. (8), it becomes

$$\left[\vec{P}^2 + (m + V_N)^2 \right] \psi = (\varepsilon - V_c)^2 \psi, \quad (24)$$

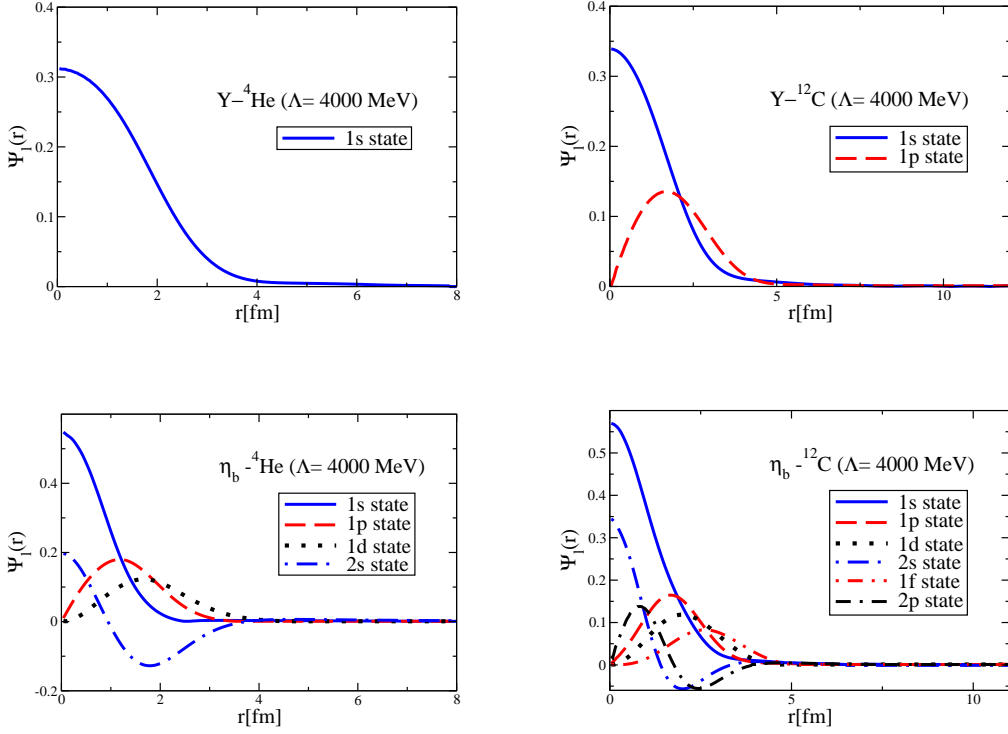


FIG. 4: Coordinate-space wave functions for the Υ - ${}^4\text{He}$ (top left), Υ - ${}^{12}\text{C}$ (top right), η_b - ${}^4\text{He}$ (bottom left) and η_b - ${}^{12}\text{C}$ (bottom right) systems for the central value of the cutoff parameter $\Lambda = 4000$ MeV.

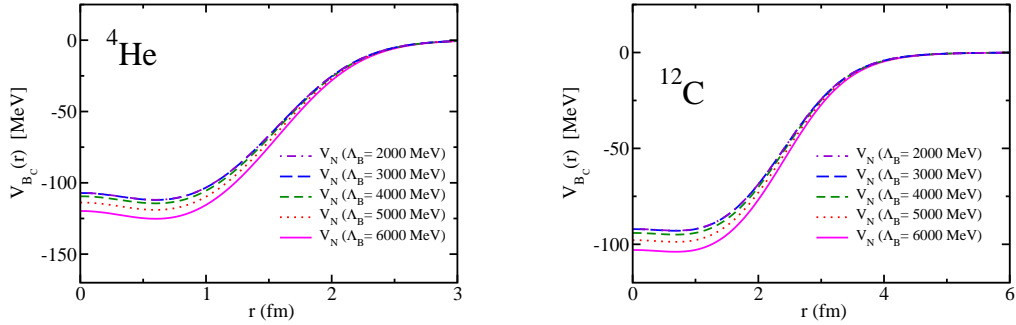


FIG. 5: Nuclear potentials for the B_c - ${}^4\text{He}$ and B_c - ${}^{12}\text{C}$ systems for different values of the cutoff parameter Λ .

and the Hamiltonian for the numerical calculation in Eq. (12) now becomes

$$\begin{aligned} \hat{H}_{ij} = & (P_i^2 + m^2)\delta_{ij} + 2mP_j^2 w_j V_{N\ell}(P_i, P_j) + \left(\sum_{k=1}^{NP} P_k^2 w_k V_{N\ell}(P_i, P_k) V_{N\ell}(P_k, P_j) \right) P_j^2 w_j \\ & + 2\varepsilon_{n\ell} P_j^2 w_j V_{c\ell}(P_i, P_j) - \left(\sum_{k=1}^{NP} P_k^2 w_k V_{c\ell}(P_i, P_k) V_{c\ell}(P_k, P_j) \right) P_j^2 w_j. \end{aligned} \quad (25)$$

The Coulomb potentials in the ${}^{12}\text{C}$ nucleus (nucleon density distribution and Coulomb mean field) is obtained within the QMC model [44] self-consistently. We show the Coulomb potentials side-by-side with the nuclear potentials for this nucleus in Fig. 7. Since the mean-field approximation of the QMC model is not good for a light nucleus such

TABLE II: ${}^4_{B_c}\text{He}$ and ${}^{12}_{B_c}\text{C}$ bound-state energies without the Coulomb potentials for the central value of the cutoff parameter $\Lambda = 4000$ MeV.

		$E_{n\ell}$ (MeV)
		$\Lambda = 4000$ MeV
${}^4_{B_c}\text{He}$	1s	-76.67
	1p	-42.91
${}^{12}_{B_c}\text{C}$	1s	-76.06
	1p	-52.88

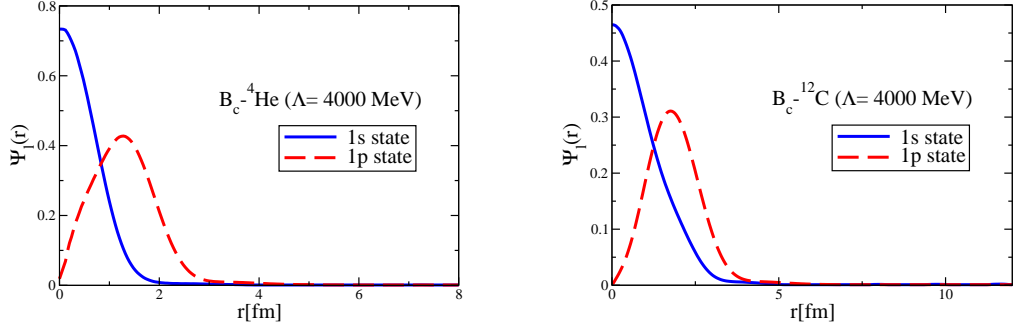


FIG. 6: Coordinate-space wave functions for the $B_c^\pm\text{-}{}^4\text{He}$ (left) and $B_c^\pm\text{-}{}^{12}\text{C}$ (right) systems without the Coulomb potentials for the central value of the cutoff parameter $\Lambda = 4000$ MeV.

as the ${}^4\text{He}$, we do not investigate the $B_c^\pm\text{-}{}^4\text{He}$ system with the Coulomb potentials in this initial study. In the near future, we plan to include the Coulomb potentials for the $B_c^\pm\text{-}{}^4\text{He}$ systems with a different approach, although the effects are expected to be small.

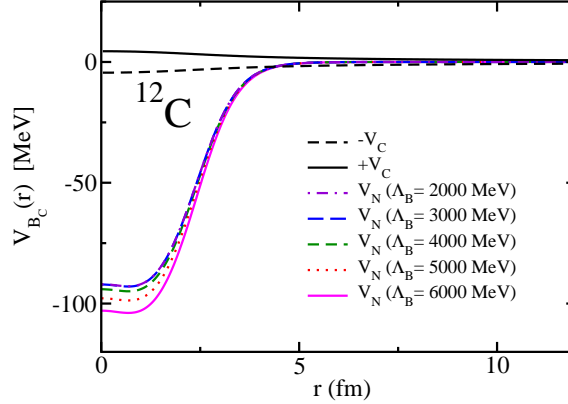


FIG. 7: Attractive and repulsive Coulomb potentials, together with the nuclear potentials for the ${}^{12}_{B_c^\pm}\text{C}$ systems.

The treatment of the Coulomb potential in momentum space is known to be difficult due to the logarithmic singularity that appears in its partial wave decomposition, requiring the use of some regularization technique, such as the Lande subtraction method [48, 51]. In the present calculation, however, the treatment is much more simple. The reason is that we can calculate the $B_c^\pm\text{-}{}^{12}\text{C}$ Coulomb potentials in coordinate space using the self-consistent mean Coulomb field in the ${}^{12}\text{C}$ nucleus by neglecting the feedback of the Coulomb force from B_c^\pm (which should give very small effects). Thus, we simply get the direct partial wave decomposition of the Coulomb potentials in momentum

TABLE III: ${}^{12}_{B_c^\pm}\text{C}$ bound-state energies with the Coulomb potentials for the central value of the cutoff parameter $\Lambda = 4000$ MeV.

$E_{n\ell}$ (MeV)	
$B_c^-{}^{12}\text{C}$ (Strong only)	
$n\ell$	$\Lambda_B = 4000$ MeV
${}^{12}_{B_c^-}\text{C}$ 1s	-76.06
1p	-52.88
$B_c^-{}^{12}\text{C}$	
$n\ell$	$\Lambda_B = 4000$
${}^{12}_{B_c^-}\text{C}$ 1s	-80.63
1p	-57.53
$B_c^-{}^{12}\text{C}$ ($2E_{V_c} \rightarrow 0$)	
$n\ell$	$\Lambda_B = 4000$
${}^{12}_{B_c^-}\text{C}$ 1s	-76.58
1p	-54.01
$B_c^+{}^{12}\text{C}$	
$n\ell$	$\Lambda_B = 4000$
${}^{12}_{B_c^+}\text{C}$ 1s	-72.53
1p	-50.49
$B_c^\pm{}^{12}\text{C}$ (Coulomb only)	
$n\ell$	$B_c^-{}^{12}\text{C}$
${}^{12}_{B_c^\pm}\text{C}$ 1s	-1.43
$n\ell$	$B_c^-{}^{12}\text{C}$ ($2E_{V_c} \rightarrow 0$)
${}^{12}_{B_c^\pm}\text{C}$ 1s	-0.01
$n\ell$	$B_c^+{}^{12}\text{C}$
${}^{12}_{B_c^\pm}\text{C}$ 1s	+1.46

space according to the method already explained in Sec. III.

We solve Eq. (24) using the direct double spherical Bessel transform for the following cases: (i) nuclear and attractive Coulomb potentials ($B_c^-{}^{12}\text{C}$), (ii) nuclear and repulsive Coulomb potentials ($B_c^+{}^{12}\text{C}$), (iii) only nuclear potentials, (iv) only Coulomb potentials, and (v) the cases of the term $2\varepsilon V_c \rightarrow 0$ in the right-hand side of Eq. (24), on the right-hand side of the expansion, $(\varepsilon - V_c)^2 = \varepsilon^2 + V_c^2 - 2\varepsilon V_c$. The results are presented in Table III (see also Table IX in Appendix A). We make this comparison to see the interference effect between the dominant strong nuclear and Coulomb potentials, which arises naturally for the relativistic K.G. equation case but not for the lowest-order Schrödinger equation. Solving Eq. (24) for $n = 1$, $\ell = 0$ and the Coulomb potential alone, we get energies, $E_{n\ell} = E_{10} \approx \pm 1.4$ MeV for $\pm|V_c|$, with a small asymmetry between the cases of the attractive and repulsive Coulomb potentials, that arises from the V_c^2 term and diminishes the energy E in both cases. Naively one could expect that the bound-state energies obtained including the nuclear and attractive (or repulsive) Coulomb potentials to be around 1.4 MeV deeper (or shallower) than the case of the nuclear potential alone, however, in fact we obtain more than 3 to 4 MeV difference for the 1s state. This happens because the nuclear potential dominates ε in the term $2\varepsilon V_c$ that appears when we include the Coulomb potential. The "interference" between the nuclear and Coulomb potentials is responsible for this larger difference. By making the term $2\varepsilon V_c \rightarrow 0$, we nearly recover the energies found for the case of only nuclear interaction, aside from a small difference due to the V_c^2 term. This shows that when including the Coulomb interaction, the nuclear potential dominates ε , as one can expect. Although the Coulomb effect is small, such behavior described above cannot be seen in a naive treatment using the Schrödinger equation without including up to the V_c^2 term.

The coordinate-space wave functions for the 1s and 1p states for the $B_c^\pm{}^{12}\text{C}$ system for the central value of the cutoff parameter $\Lambda = 4000$ MeV are presented in Fig. 8.

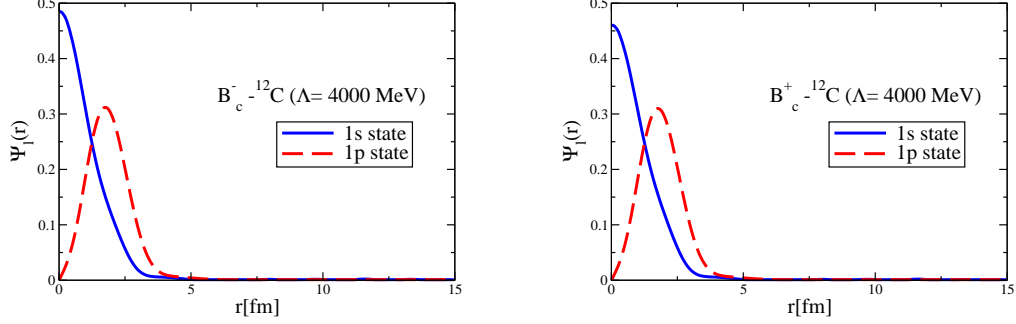


FIG. 8: Coordinate-space wave functions for 1s and 1p states of the $B_c^- -^{12}\text{C}$ (left) and $B_c^+ -^{12}\text{C}$ (right) systems for the central value of the cutoff parameter $\Lambda = 4000$ MeV.

VII. SUMMARY AND CONCLUSION

By solving the Klein-Gordon equation in momentum space, we have calculated the single-particle energies and the corresponding coordinate-space wave functions for the quarkonium-nucleus systems, for the Υ and η_b mesons and the ^4He and ^{12}C nuclei. The meson-nucleus potentials have been calculated from the mass shift amount of the mesons in nuclear matter using a local density approximation without the effects of the meson widths. The results depend on the cutoff parameter Λ values, introduced in the regularization of the meson self-energy calculations.

We also have calculated for the first time the $B_c^- - ^4\text{He}$ and $B_c^- - ^{12}\text{C}$ bound-state energies and coordinate-space wave functions, with only the strong interaction potentials first, and then, for the $B_c^\pm - ^{12}\text{C}$ system, we have studied including the realistic Coulomb potentials, and analyzed the "interference" effect between the nuclear and Coulomb potentials.

In the future, more realistic studies can be made for the Υ^- , η_b^- and B_c^\pm -nucleus systems for various nuclei, including the possible imaginary part of the potentials (widths) for the Υ^- , η_b^- and B_c^\pm -nucleus bound states. In particular, the realistic Coulomb potentials will be included for the B_c^\pm - and $B_c^{*\pm}$ -nucleus systems.

Acknowledgments

The authors acknowledge the support and warm hospitality of Asia Pacific Center for Theoretical Physics (APCTP) during the Workshop (APCTP PROGRAMS 2023) "Origin of Matter and Masses in the Universe: Hadrons in free space, dense nuclear medium, and compact stars," where important discussions and development were achieved on the topic. The authors also thank the Origin of Matter and Evolution of Galaxies Institute at Soongsil University for the supports in many aspects during the collaboration visit in Korea. The authors thank A. W. Thomas for his useful comments on the coordinate space wave functions at the initial stage of the study and fruitful discussions on this topic. G.N.Z. was supported by the Coordenação de Aperfeiçoamento de Pessoal de Nível Superior-Brazil (CAPES). JJCM acknowledges financial support from the University of Sonora under Grant No. USO315009105. K.T. was supported by Conselho Nacional de Desenvolvimento Científico e Tecnológico (CNPq, Brazil), Processes No. 313063/2018-4, No. 426150/2018-0, and No. 304199/2022-2, and FAPESP Process No. 2019/00763-0 and No. 2023/073-3-6 (G.N.Z. and K.T.). The work of G.N.Z and K.T. was in the projects of Instituto Nacional de Ciência e Tecnologia - Nuclear Physics and Applications (INCT-FNA), Brazil, Process No. 464898/2014-5.

-
- [1] G. Krein, A. W. Thomas and K. Tsushima, Phys. Lett. B **697** (2011), 136.
 - [2] K. Tsushima, D. H. Lu, G. Krein and A. W. Thomas, Phys. Rev. C **83** (2011), 065208.
 - [3] C. M. Ko, P. Levai, X. J. Qiu and C. T. Li, Phys. Rev. C **45** (1992), 1400.
 - [4] M. Asakawa, C. M. Ko, P. Levai and X. J. Qiu, Phys. Rev. C **46** (1992) R1159.
 - [5] E. Friedman and G. Soff, J. Phys. G **11**, L37 (1985).
 - [6] Yamazaki, T., Hayano, R.S., Itahashi, K. et al., Z. Physik A — Hadrons and Nuclei 355, 219 (1996).
 - [7] R. S. Hayano, S. Hirezaki and A. Gillitzer, Eur. Phys. J. A **6**, 99 (1999).
 - [8] K. Tsushima, D. H. Lu, A. W. Thomas and K. Saito, Phys. Lett. B **443**, 26 (1998).

- [9] K. Tsushima, D. H. Lu, A. W. Thomas, K. Saito and R. H. Landau, *Phys. Rev. C* **59**, 2824 (1999).
- [10] S. J. Brodsky, I. A. Schmidt and G. F. de Teramond, *Phys. Rev. Lett.* **64** (1990), 1011.
- [11] A. Hosaka, T. Hyodo, K. Sudoh, Y. Yamaguchi and S. Yasui, *Prog. Part. Nucl. Phys.* **96** (2017), 88.
- [12] V. Metag, M. Nanova and E. Y. Paryev, *Prog. Part. Nucl. Phys.* **97** (2017), 199.
- [13] G. Krein, A. W. Thomas and K. Tsushima, *Prog. Part. Nucl. Phys.* **100** (2018), 161.
- [14] S. H. Lee and C. M. Ko, *Phys. Rev. C* **67** (2003), 038202.
- [15] G. Krein, *J. Phys. Conf. Ser.* **422** (2013), 012012.
- [16] F. Klingl, S. s. Kim, S. H. Lee, P. Morath and W. Weise, *Phys. Rev. Lett.* **82** (1999), 3396; **83** (1999), 4224.
- [17] A. Hayashigaki, *Prog. Theor. Phys.* **101** (1999), 923.
- [18] A. Kumar and A. Mishra, *Phys. Rev. C* **82** (2010), 045207.
- [19] V. B. Belyaev, N. V. Shevchenko, A. I. Fix and W. Sandhas, *Nucl. Phys. A* **780** (2006), 100.
- [20] A. Yokota, E. Hiyama and M. Oka, *PTEP* **2013** (2013), 113D01.
- [21] M. E. Peskin, *Nucl. Phys. B* **156** (1979), 365.
- [22] D. Kharzeev, *Proc. Int. Sch. Phys. Fermi* **130** (1996), 105.
- [23] A. B. Kaidalov and P. E. Volkovitsky, *Phys. Rev. Lett.* **69** (1992), 3155.
- [24] M. E. Luke, A. V. Manohar and M. J. Savage, *Phys. Lett. B* **288** (1992), 355.
- [25] G. F. de Teramond, R. Espinoza and M. Ortega-Rodriguez, *Phys. Rev. D* **58** (1998), 034012.
- [26] S. J. Brodsky and G. A. Miller, *Phys. Lett. B* **412** (1997), 125.
- [27] A. Sibirtsev and M. B. Voloshin, *Phys. Rev. D* **71** (2005), 076005.
- [28] M. B. Voloshin, *Prog. Part. Nucl. Phys.* **61** (2008), 455.
- [29] J. Tarrús Castellà and G. Krein, *Phys. Rev. D* **98** (2018), 014029.
- [30] J. J. Cobos-Martínez, K. Tsushima, G. Krein and A. W. Thomas, *Phys. Lett. B* **811** (2020), 135882.
- [31] K. Yokokawa, S. Sasaki, T. Hatsuda and A. Hayashigaki, *Phys. Rev. D* **74** (2006), 034504.
- [32] T. Kawanai and S. Sasaki, *Phys. Rev. D* **82** (2010), 091501.
- [33] U. Skerbis and S. Prelovsek, *Phys. Rev. D* **99** (2019), 094505.
- [34] E. Chizzali, Y. Kamiya, R. Del Grande, T. Doi, L. Fabbietti, T. Hatsuda and Y. Lyu, *Phys. Lett. B* **848** (2024), 138358.
- [35] F. Etminan and A. Aalimi, *Phys. Rev. C* **109**, 054002 (2024).
- [36] G. N. Zeminiani, J. J. Cobos-Martinez and K. Tsushima, *Eur. Phys. J. A* **57**, 259 (2021).
- [37] G. N. Zeminiani, [arXiv:2201.09158 [nucl-th]].
- [38] G. Zeminiani, J. J. Cobos-Martínez and K. Tsushima, *PoS PANIC2021* (2022), 208.
- [39] J. J. Cobos-Martínez, G. N. Zeminiani and K. Tsushima, *Phys. Rev. C* **105**, 025204 (2022).
- [40] P. A. Guichon, *Phys. Lett. B* **200**, 235 (1988).
- [41] P. A. M. Guichon, K. Saito, E. N. Rodionov and A. W. Thomas, *Nucl. Phys. A* **601**, 349 (1996).
- [42] K. Tsushima and F. Khanna, *Phys. Lett. B* **552**, 138 (2003).
- [43] K. Tsushima, K. Saito, A. W. Thomas and S. V. Wright, *Phys. Lett. B* **429**, 239 (1998); *Phys. Lett. B* **436**, 453(E) (1998).
- [44] K. Saito, K. Tsushima and A. W. Thomas, *Nucl. Phys. A* **609**, 339 (1996).
- [45] K. Saito, K. Tsushima and A. W. Thomas, *Prog. Part. Nucl. Phys.* **58**, 1 (2007).
- [46] K. Tsushima, *AAPPS* **29**, 37 (2019).
- [47] K. Saito, K. Tsushima and A. W. Thomas, *Phys. Rev. C* **56**, 566 (1997).
- [48] D. P. Heddle, Y. R. Kwon and F. Tabakin, *Comput. Phys. Commun.* **38**, 71 (1985).
- [49] Y. R. Kwon, *Hadronic atoms in momentum space*, Ph.D. thesis, University of Pittsburgh, 1978.
- [50] G. N. Zeminiani, S. L. P. G. Beres and K. Tsushima, *Phys. Rev. D* **110**, 094045 (2024).
- [51] Y. R. Kwon and F. Tabakin, *Phys. Rev. C* **18**, 932 (1978).

Appendix A: Results comparison

The treatment in momentum space requires the nuclear potentials to be transformed from coordinate space to momentum space, and then decomposed into partial waves. For this purpose we compare three different methods, namely, (i) the spherical Bessel transform of the numerically obtained original potential in coordinate space, (ii) the partial wave decomposition of the Fourier transform of the Woods-Saxon approximated form for the original potential, and (iii) the spherical Bessel transform of the Woods-Saxon approximation of the numerically obtained original potential. The spherical Bessel transform of the numerically obtained original potential was already explained in Sec. III.

In order to use conveniently the approximated form for the calculated quarkonium-nucleus potentials shown in Fig. 3, we adopt the Woods-Saxon potential form which is commonly used to approximately parameterize nuclear potentials,

$$V_{WS}(r = |\vec{r}|) = -\frac{V_0}{1 + e^{(r-R)/a}}, \quad (\text{A1})$$

where $V_0(> 0)$ is the potential depth, R is the nuclear radius and a is the surface thickness of the nucleus. These parameters will be determined by the fit for each nucleus for a given numerically obtained original potential.

The use of the Woods-Saxon form parameterized potential enables us to work with an analytical form of $V_N(r)$. This is done by interpolating the numerical data to fit to the Woods-Saxon shape. The obtained parameters for each potential are presented in Tables IV and V. The advantage of using the Woods-Saxon potential form is that, one does not need to be provided with the obtained original numerical potential data, but just may know the Woods-Saxon potential parameters.

TABLE IV: Parameters of the fitted Woods-Saxon form potentials for the $V_{\Upsilon-4\text{He}}$, $V_{\Upsilon-12\text{C}}$, $V_{\eta_b-4\text{He}}$, and $V_{\eta_b-12\text{C}}$ potentials and different cutoff values.

		Woods-Saxon potential parameter values		
		$\Lambda_B = 2000 \text{ MeV}$	$\Lambda_B = 4000 \text{ MeV}$	$\Lambda_B = 6000 \text{ MeV}$
$V_{\Upsilon-4\text{He}}$	$V_0 \text{ (MeV)}$	19.83	22.84	27.54
	$R \text{ (fm)}$	1.6199	1.6215	1.6237
	$a \text{ (fm)}$	0.2832	0.2833	0.2835
$V_{\Upsilon-12\text{C}}$	$V_0 \text{ (MeV)}$	16.66	19.21	23.20
	$R \text{ (fm)}$	2.4638	2.4662	2.4692
	$a \text{ (fm)}$	0.4805	0.4806	0.4808
$V_{\eta_b-4\text{He}}$	$V_0 \text{ (MeV)}$	91.84	95.91	101.42
	$R \text{ (fm)}$	1.6351	1.6352	1.6353
	$a \text{ (fm)}$	0.28445	0.28446	0.28447
$V_{\eta_b-12\text{C}}$	$V_0 \text{ (MeV)}$	77.82	81.28	85.96
	$R \text{ (fm)}$	2.4854	2.4856	2.4858
	$a \text{ (fm)}$	0.48181	0.48182	0.48183

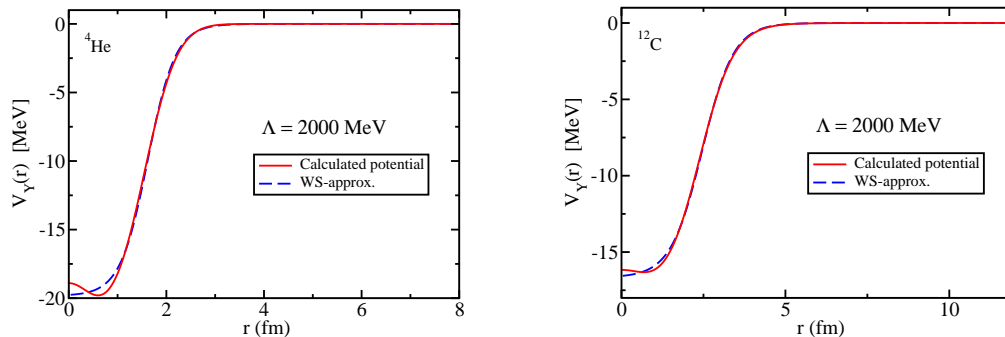
A comparison between the numerically obtained original potentials and the corresponding fitted Woods-Saxon form potentials is made in Fig. 9 for $V_{\Upsilon-4\text{He}}$ and $V_{\Upsilon-12\text{C}}$ for the case of $\Lambda = 2000 \text{ MeV}$. One can easily observe that the fitted Woods-Saxon form potentials are good approximations of the original potentials, and the differences in the calculated bound state energies using the parametrized potentials are expected to be small (indeed, this will be demonstrated later).

The Fourier transform of the Woods-Saxon form potential of Eq. (A1) can be carried out analytically using complex analysis. After the integration in the complex plane, we end up with the following equation

$$V_{WS}(\vec{P}, \vec{P}') = -\frac{V_0}{2\pi^2} \frac{a^2}{|\vec{P} - \vec{P}'|} \left\{ \frac{2\pi e^{-\pi\rho}}{(1 - e^{-2\pi\rho})^2} \left[\pi (1 - e^{-2\pi\rho}) \sin(\alpha\rho) - \alpha (1 - e^{-2\pi\rho}) \cos(\alpha\rho) \right] \right. \\ \left. - 2 \sum_{n=0}^{n_{max}} (-1)^n \gamma^n \frac{n\rho}{(\rho^2 + n^2)} \right\}, \quad (\text{A2})$$

TABLE V: Parameters of the fitted Woods-Saxon shape for the $V_{B_c-^4\text{He}}$ and $V_{B_c-^{12}\text{C}}$ potentials and different cutoff values.

		Woods-Saxon potential parameter values		
		$\Lambda_B = 2000$ MeV	$\Lambda_B = 4000$ MeV	$\Lambda_B = 6000$ MeV
$V_{B_c-^4\text{He}}$	V_0 (MeV)	112.12	114.61	125.45
	R (fm)	1.6308	1.6311	1.6307
	a (fm)	0.28427	0.2843	0.28426
$V_{B_c-^{12}\text{C}}$	V_0 (MeV)	94.77	96.90	106.04
	R (fm)	2.4796	2.4801	2.4795
	a (fm)	0.48167	0.4817	0.48166

FIG. 9: Comparison between the originally obtained Υ -nucleus potentials (solid line) and the fitted Woods-Saxon potentials (long-dashed line) for ^4He (left) and ^{12}C (right) for the cutoff $\Lambda = 2000$ MeV.

with $\rho = (|\vec{P} - \vec{P}'|)a$, $\alpha = R/a$ and $\gamma = e^{-\alpha}$. The value of n_{max} does not affect significantly the final result, since the first few terms in the sum already gives nearly a converged result, and thus $n_{max} = 4$ or 5 is sufficient.

The partial wave ℓ -projected potentials in momentum space are then calculated by

$$V_{N\ell}(P, P') = 2\pi \int_{-1}^1 d\cos\theta P_\ell(\cos\theta) V_{WS}(\vec{P}, \vec{P}'), \quad (\text{A3})$$

where P_ℓ are the Legendre polynomials of ℓ th order and θ is the angle between \vec{P} and \vec{P}' . After the Fourier transform is performed analytically, the partial wave decomposition is made numerically.

The results obtained by the different methods of partial wave decomposition and different values of the cutoff values are presented in Tables VI to IX. The wave functions are presented in Figs. 10 to 28.

The three methods discussed above and the cutoff dependence in the nuclear potential give slightly different results for the bound-state energies and wave functions of the meson-nucleus systems considered. However, we emphasize that these differences do not change the conclusion that the studied meson-nucleus systems should form bound states based on the strong potentials.

We compare in Fig. 29 the wave functions of the 1s state of the Υ - ^{12}C system for different cutoff values and methods. Although the bound-state energies of the 1s energy level varies slightly according to the cutoff values or the method used, the wave functions obtained show very similar shapes and amplitudes.

Appendix B: Numerical precision

In Table B we compare the bound-state energies of the 1s state of the Υ - ^{12}C system for different maximum error acceptances in the convergence of the results and number of grid points used in the numerical integrations. We see that the results are numerically consistent within each method. (See Table VI for comparison.)

TABLE VI: ${}^4_{\Upsilon}\text{He}$ and ${}^{12}_{\Upsilon}\text{C}$ bound-state energies, obtained by the Direct Bessel [Eq. (9)], Woods-Saxon Fourier [Eqs. (A2) and (A3)] and Woods-Saxon Bessel [Eqs. (A1) and (9)] transform methods. The Λ_B values are in MeV.

		Bound state energies (MeV)		
		Direct Bessel transform		
$n\ell$		$\Lambda_B = 2000$	$\Lambda_B = 4000$	$\Lambda_B = 6000$
${}^4_{\Upsilon}\text{He}$	1s	-5.93	-6.25	-6.56
${}^{12}_{\Upsilon}\text{C}$	1s	-13.22	-15.26	-18.41
	1p	-8.30	-9.57	-11.51
		Woods-Saxon Fourier transform		
$n\ell$		$\Lambda_B = 2000$	$\Lambda_B = 4000$	$\Lambda_B = 6000$
${}^4_{\Upsilon}\text{He}$	1s	-5.48	-7.4	-10.6
${}^{12}_{\Upsilon}\text{C}$	1s	-10.51	-12.67	-16.1
	1p	-5.95	-7.79	-10.78
		Woods-Saxon Bessel transform		
$n\ell$		$\Lambda_B = 2000$	$\Lambda_B = 4000$	$\Lambda_B = 6000$
${}^4_{\Upsilon}\text{He}$	1s	-6.35	-6.75	-7.14
${}^{12}_{\Upsilon}\text{C}$	1s	-13.18	-15.22	-18.37
	1p	-8.18	-9.43	-11.33

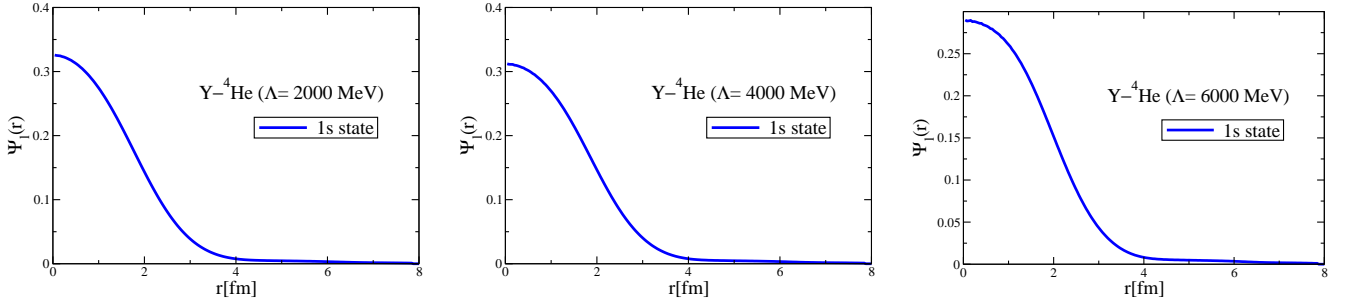


FIG. 10: Coordinate-space 1s state wave functions of the ${}^4_{\Upsilon}\text{He}$ system for different values of cutoff Λ obtained by the direct Bessel transform.

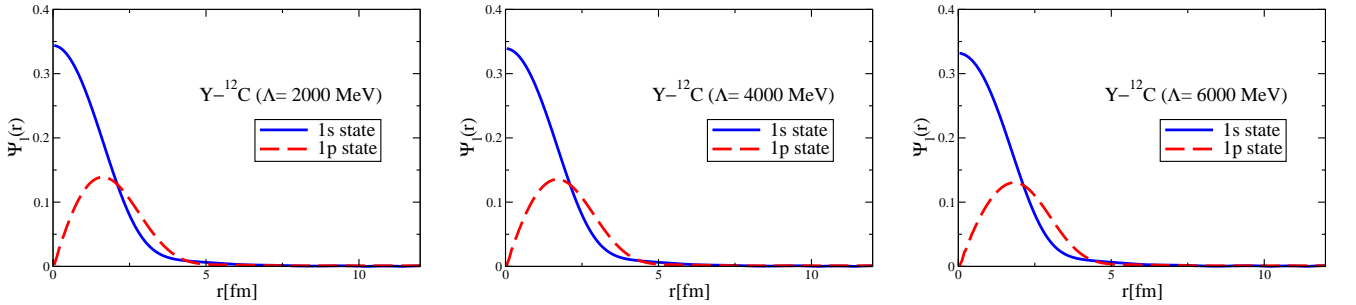


FIG. 11: Coordinate-space 1s and 1p state wave functions of the ${}^{12}_{\Upsilon}\text{C}$ system for different values of cutoff Λ obtained by the direct Bessel transform.

TABLE VII: ${}^4_{\eta_b}\text{He}$ and ${}^{12}_{\eta_b}\text{C}$ bound-state energies, obtained by the Direct Bessel [Eq. (9)], Woods-Saxon Fourier [Eqs. (A2) and (A3)] and Woods-Saxon Bessel [Eqs. (A1) and (9)] transform methods. The Λ_B values are in MeV.

		Bound state energies (MeV)		
		Direct Bessel transform		
$n\ell$		$\Lambda_B = 2000$	$\Lambda_B = 4000$	$\Lambda_B = 6000$
${}^4_{\eta_b}\text{He}$	1s	-68.71	-71.59	-75.44
	1p	-39.97	-41.50	-43.54
	1d	-37.73	-39.56	-42.03
	2s	-29.14	-30.09	-31.38
${}^{12}_{\eta_b}\text{C}$	1s	-63.70	-66.93	-70.27
	1p	-53.17	-55.13	-59.38
	1d	-46.47	-48.50	-51.17
	2s	-34.53	-36.30	-39.43
	1f	-26.56	-28.09	-29.97
	2p	-18.86	-20.67	-23.15
		Woods-Saxon Fourier transform		
$n\ell$		$\Lambda_B = 2000$	$\Lambda_B = 4000$	$\Lambda_B = 6000$
${}^4_{\eta_b}\text{He}$	1s	-63.1	-66.7	-71.5
	1p	-40.6	-43.7	-48.0
	1d	-17.2	-19.7	-23.2
	2s	-15.6	-17.9	-21.1
${}^{12}_{\eta_b}\text{C}$	1s	-65.8	-69.0	-73.4
	1p	-57.0	-60.1	-64.3
	1d	-47.5	-50.4	-54.4
	2s	-46.3	-49.1	-53.0
	1f	-37.5	-40.2	-43.9
	2p	-36.0	-38.6	-42.2
		Woods-Saxon Bessel transform		
$n\ell$		$\Lambda_B = 2000$	$\Lambda_B = 4000$	$\Lambda_B = 6000$
${}^4_{\eta_b}\text{He}$	1s	-67.79	-70.65	-74.48
	1p	-40.42	-41.95	-43.99
	1d	-36.46	-38.23	-40.64
	2s	-28.67	-29.60	-30.85
${}^{12}_{\eta_b}\text{C}$	1s	-63.41	-66.05	-69.59
	1p	-52.90	-55.44	-58.87
	1d	-46.34	-48.35	-51.05
	2s	-34.12	-36.41	-39.54
	1f	-26.90	-28.29	-30.18
	2p	-18.72	-20.53	-23.02

TABLE VIII: ${}^4_{B_c}\text{He}$ and ${}^{12}_{B_c}\text{C}$ bound-state energies without the Coulomb potentials, obtained by the Direct Bessel [Eq. (9)], Woods-Saxon Fourier [Eqs. (A2) and (A3)] and Woods-Saxon Bessel [Eqs. (A1) and (9)] transform methods. The Λ_B values are in MeV.

		Bound state energies (MeV)		
		Direct Bessel transform		
$n\ell$		$\Lambda_B = 2000$	$\Lambda_B = 4000$	$\Lambda_B = 6000$
${}^4_{B_c}\text{He}$	1s	-75.14	-76.67	-83.14
	1p	-42.06	-42.91	-46.43
${}^{12}_{B_c}\text{C}$	1s	-74.55	-76.06	-82.43
	1p	-51.53	-52.88	-58.64
		Woods-Saxon Fourier transform		
$n\ell$		$\Lambda_B = 2000$	$\Lambda_B = 4000$	$\Lambda_B = 6000$
${}^4_{B_c}\text{He}$	1s	-78.04	-80.22	-89.68
	1p	-51.42	-53.34	-61.68
${}^{12}_{B_c}\text{C}$	1s	-79.67	-81.65	-90.14
	1p	-68.62	-70.50	-78.57
		Woods-Saxon Bessel transform		
$n\ell$		$\Lambda_B = 2000$	$\Lambda_B = 4000$	$\Lambda_B = 6000$
${}^4_{B_c}\text{He}$	1s	-74.10	-75.53	-82.09
	1p	-42.43	-43.26	-46.75
${}^{12}_{B_c}\text{C}$	1s	-74.31	-75.83	-82.21
	1p	-51.79	-53.19	-58.93

TABLE IX: ${}^{12}_{B_c^\pm}\text{C}$ bound-state energies with the Coulomb potentials, obtained by the Direct Bessel [Eq. (9)] transform method. The Λ_B values are in MeV.

		Bound state energies (MeV)		
		$B_c^-{}^{12}\text{C}$ (Strong only)		
$n\ell$		$\Lambda_B = 2000$	$\Lambda_B = 4000$	$\Lambda_B = 6000$
${}^{12}_{B_c}\text{C}$	1s	-74.55	-76.06	-82.43
	1p	-51.53	-52.88	-58.64
		$B_c^-{}^{12}\text{C}$		
$n\ell$		$\Lambda_B = 2000$	$\Lambda_B = 4000$	$\Lambda_B = 6000$
${}^{12}_{B_c}\text{C}$	1s	-79.12	-80.63	-87.03
	1p	-56.15	-57.53	-63.38
		$B_c^-{}^{12}\text{C}$ ($2E_{V_c} \rightarrow 0$)		
$n\ell$		$\Lambda_B = 2000$	$\Lambda_B = 4000$	$\Lambda_B = 6000$
${}^{12}_{B_c}\text{C}$	1s	-75.06	-76.58	-82.98
	1p	-52.63	-54.01	-59.85
		$B_c^+{}^{12}\text{C}$		
$n\ell$		$\Lambda_B = 2000$	$\Lambda_B = 4000$	$\Lambda_B = 6000$
${}^{12}_{B_c^+}\text{C}$	1s	-71.01	-72.53	-78.94
	1p	-49.11	-50.49	-56.32
		$B_c^\pm{}^{12}\text{C}$ (Coulomb only)		
$n\ell$		$B_c^-{}^{12}\text{C}$	$B_c^-{}^{12}\text{C}$ ($2E_{V_c} \rightarrow 0$)	$B_c^+{}^{12}\text{C}$
${}^{12}_{B_c^\pm}\text{C}$	1s	-1.43	-0.01	+1.46

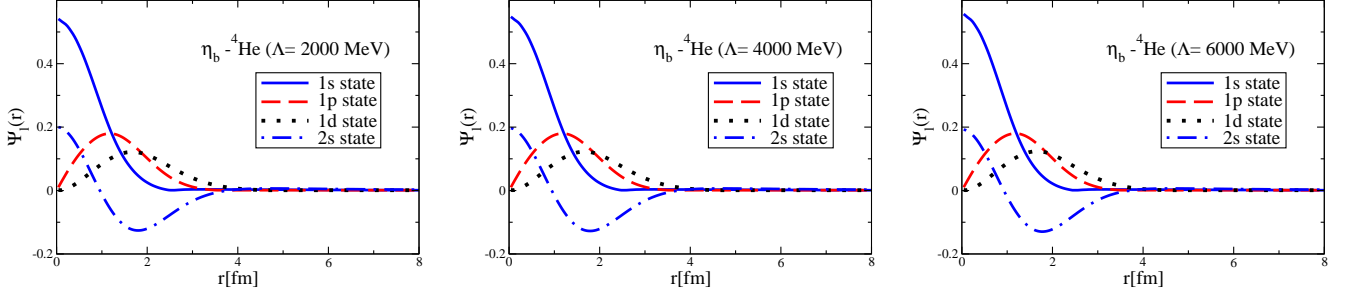


FIG. 12: Coordinate-space wave functions for the 1s to 2s states of the $\eta_b^{-4}\text{He}$ system for different values of cutoff Λ obtained by the direct Bessel transform.

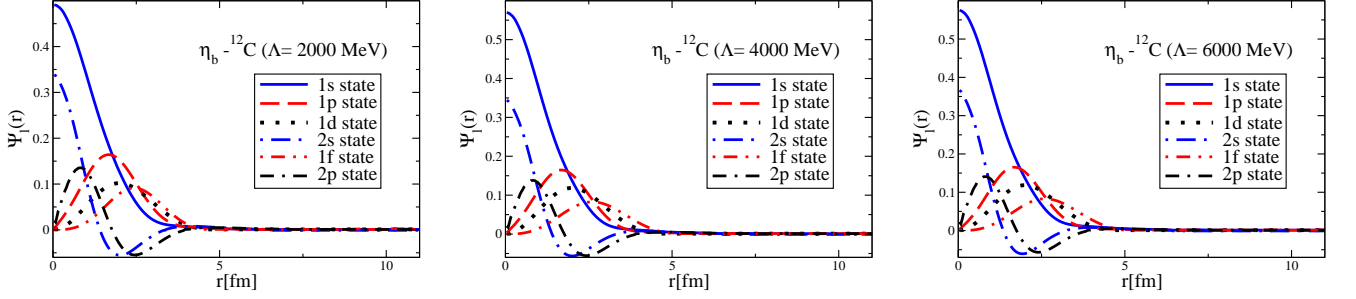


FIG. 13: Coordinate-space wave functions for the 1s to 2p states of the $\eta_b^{-12}\text{C}$ system for different values of cutoff Λ obtained by the direct Bessel transform.

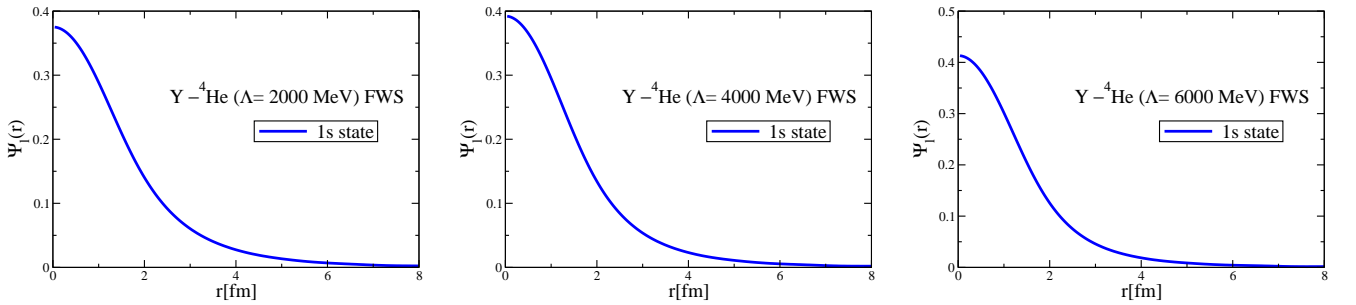


FIG. 14: Coordinate-space 1s state wave functions of the $\Upsilon^{-4}\text{He}$ system for different values of cutoff Λ obtained by the Fourier transform of the fitted Woods-Saxon form potential.

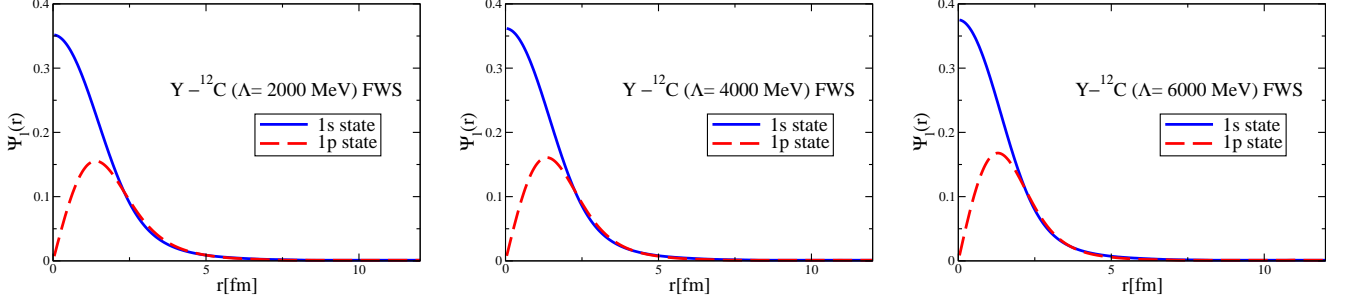


FIG. 15: Coordinate-space 1s and 1p state wave functions of the Υ - ^{12}C system for different values of cutoff Λ obtained by the Fourier transform of the fitted Woods-Saxon form potential.

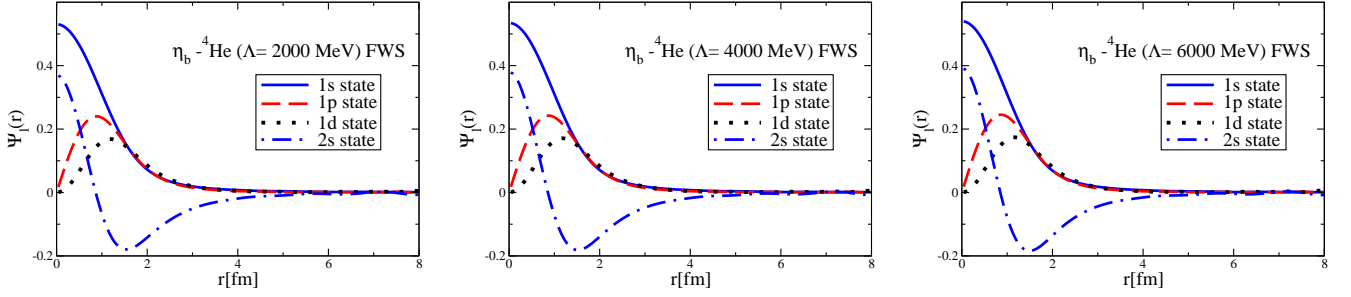


FIG. 16: Coordinate-space wave functions for the 1s to 2s states of the η_b - ^4He system for different values of cutoff Λ obtained by the Fourier transform of the fitted Woods-Saxon form potential.

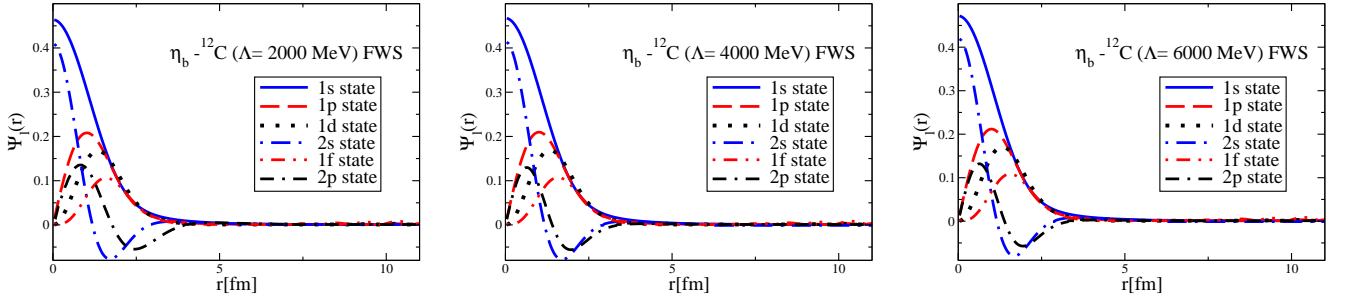


FIG. 17: Coordinate-space wave functions for the 1s to 2p states of the η_b - ^{12}C system for different values of cutoff Λ obtained by the Fourier transform of the fitted Woods-Saxon form potential.

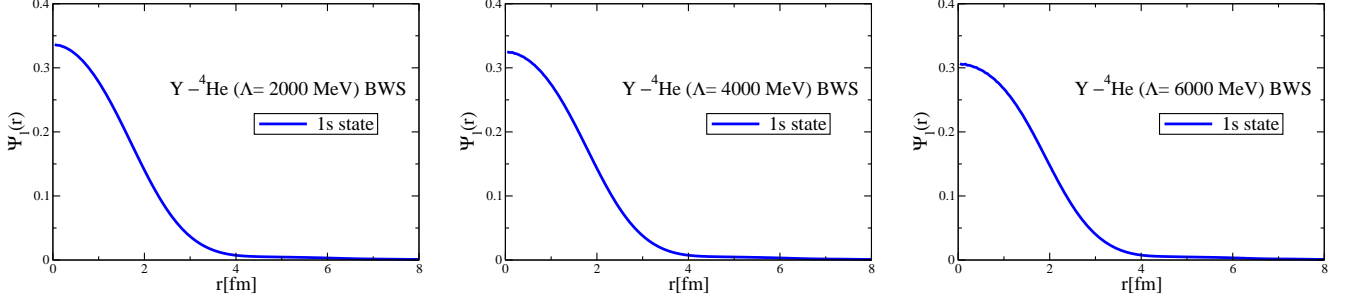


FIG. 18: Coordinate-space 1s state wave functions of the Υ - ${}^4\text{He}$ system for different values of cutoff Λ obtained by the spherical Bessel transform of the fitted Woods-Saxon form potential.

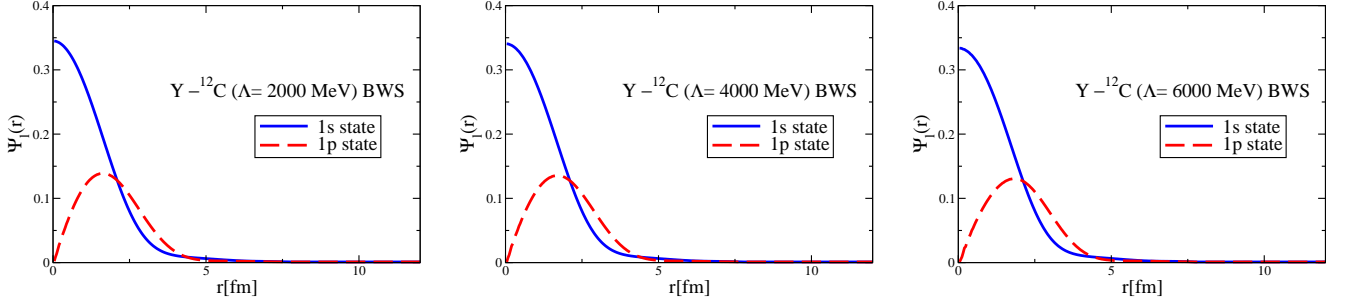


FIG. 19: Coordinate-space 1s and 1p state wave functions of the Υ - ${}^{12}\text{C}$ system for different values of cutoff Λ obtained by the spherical Bessel transform of the fitted Woods-Saxon form potential.

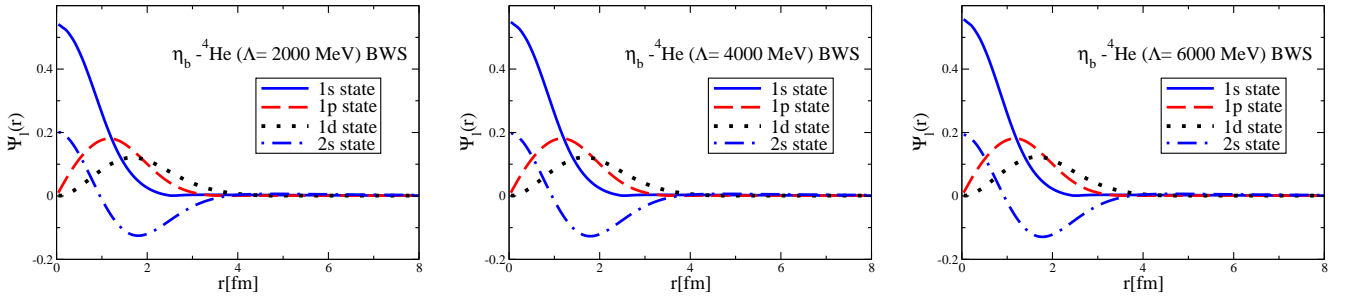


FIG. 20: Coordinate-space wave functions for the 1s to 2s states of the η_b - ${}^4\text{He}$ system for different values of cutoff Λ obtained by the spherical Bessel transform of the fitted Woods-Saxon form potential.

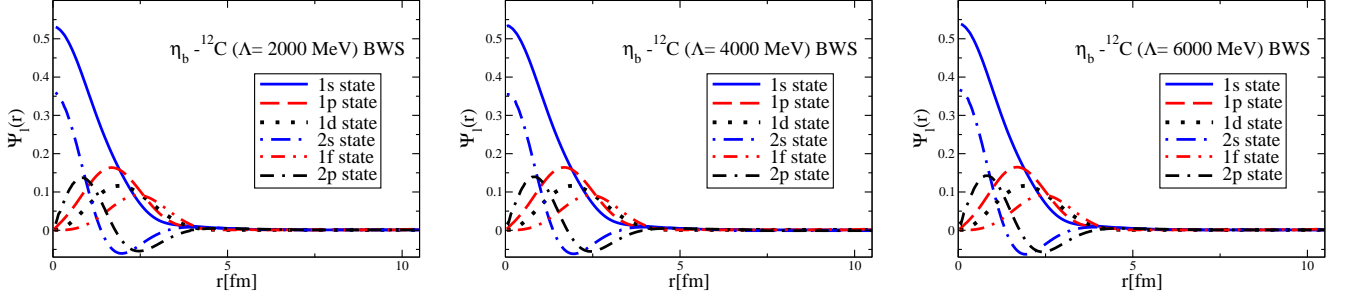


FIG. 21: Coordinate-space wave functions for the 1s to 2p states of the η_b - ^{12}C system for different values of cutoff Λ obtained the spherical Bessel transform of the fitted Woods-Saxon form potential.

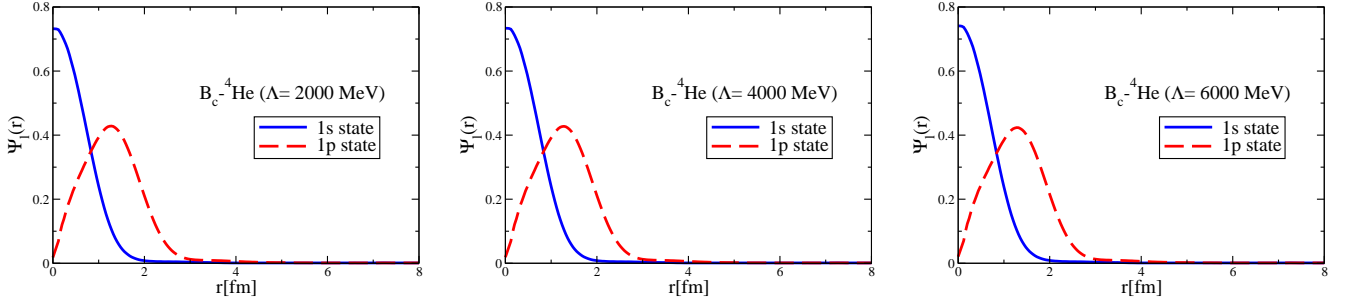


FIG. 22: Wave functions for the 1s and 1p states of the B_c - ^4He system without the Coulomb potentials for different values of Λ calculated using the direct Bessel transform.

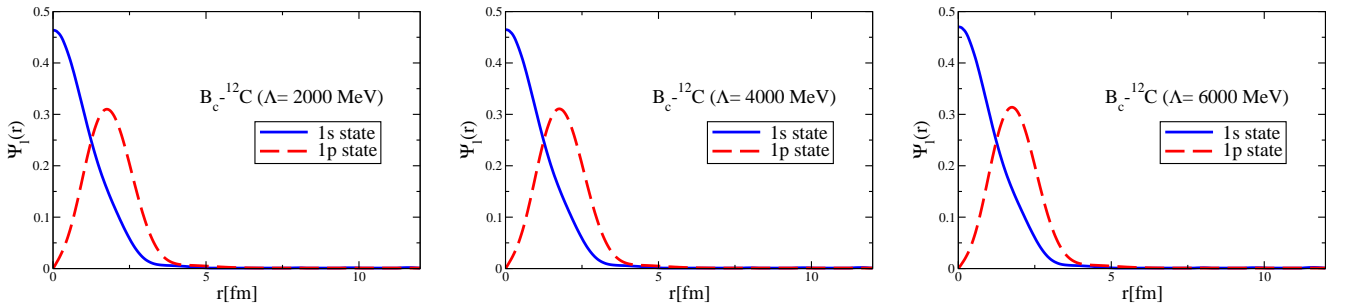


FIG. 23: Coordinate-space wave functions for the 1s and 1p states of the B_c - ^{12}C system without the Coulomb potentials for different values of Λ calculated using the direct Bessel transform.

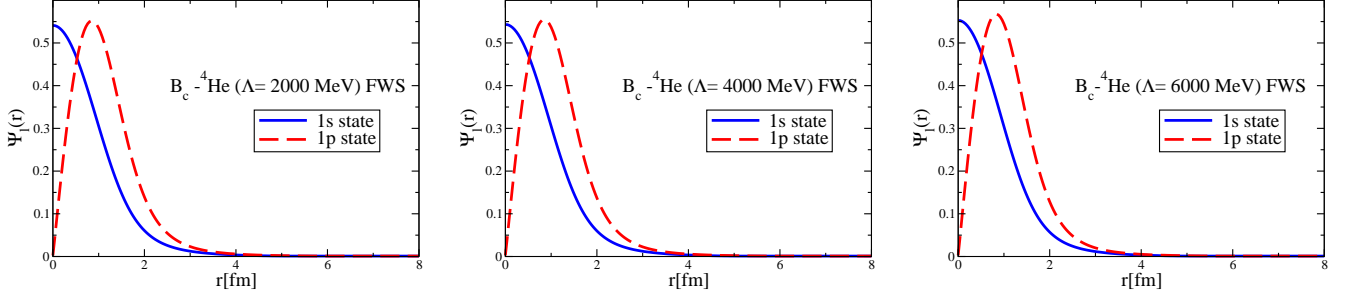


FIG. 24: Coordinate-space wave functions for the 1s and 1p states of the $B_c^{-4}\text{He}$ system without the Coulomb potentials for different values of Λ calculated using the Fourier transform of the fitted Woods-Saxon form potential.

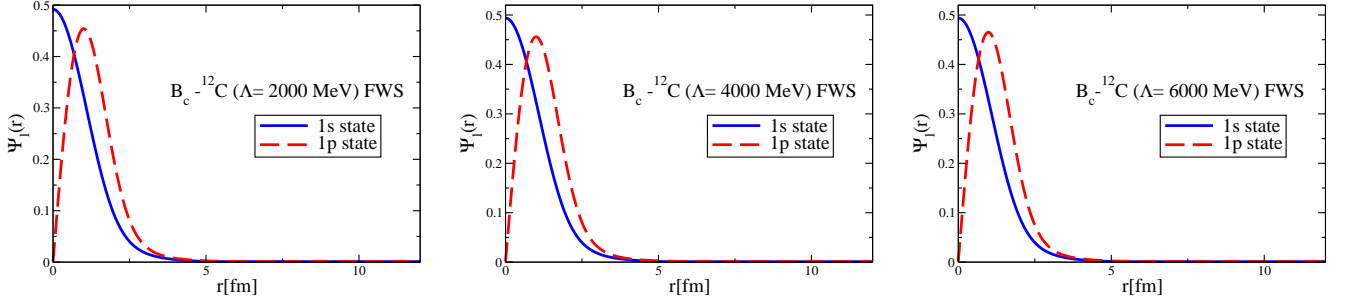


FIG. 25: Coordinate-space wave functions for the 1s and 1p states of the $B_c^{-12}\text{C}$ system without the Coulomb potentials for different values of Λ calculated using the Fourier transform of the fitted Woods-Saxon form potential.

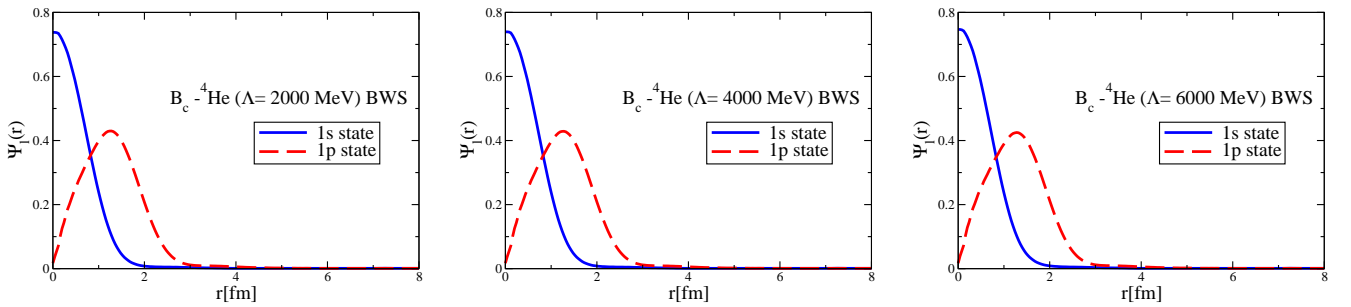


FIG. 26: Coordinate-space wave functions of the 1s and 1p states of the $B_c^{-4}\text{He}$ system without the Coulomb potentials for different values of Λ calculated using the spherical Bessel transform of the fitted Woods-Saxon form potential.

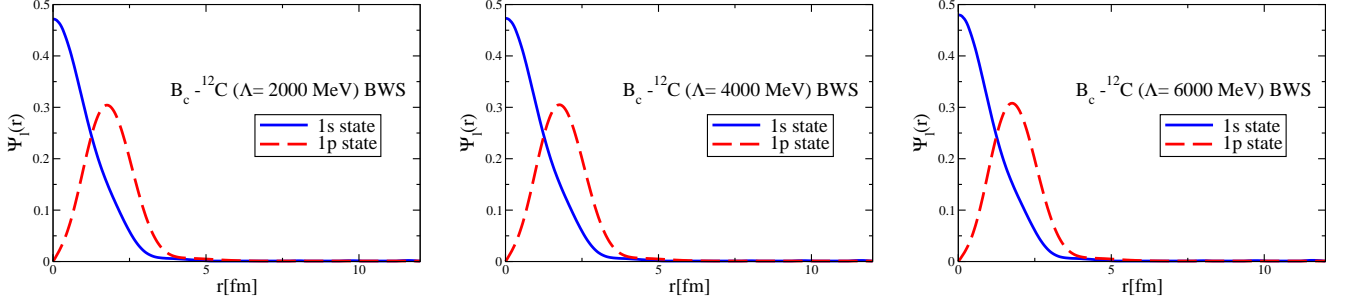


FIG. 27: Coordinate-space wave functions for the 1s and 1p states of the $B_c^-{}^{12}\text{C}$ system without the Coulomb potentials for different values of Λ calculated using the spherical Bessel transform of the fitted Woods-Saxon form potential.

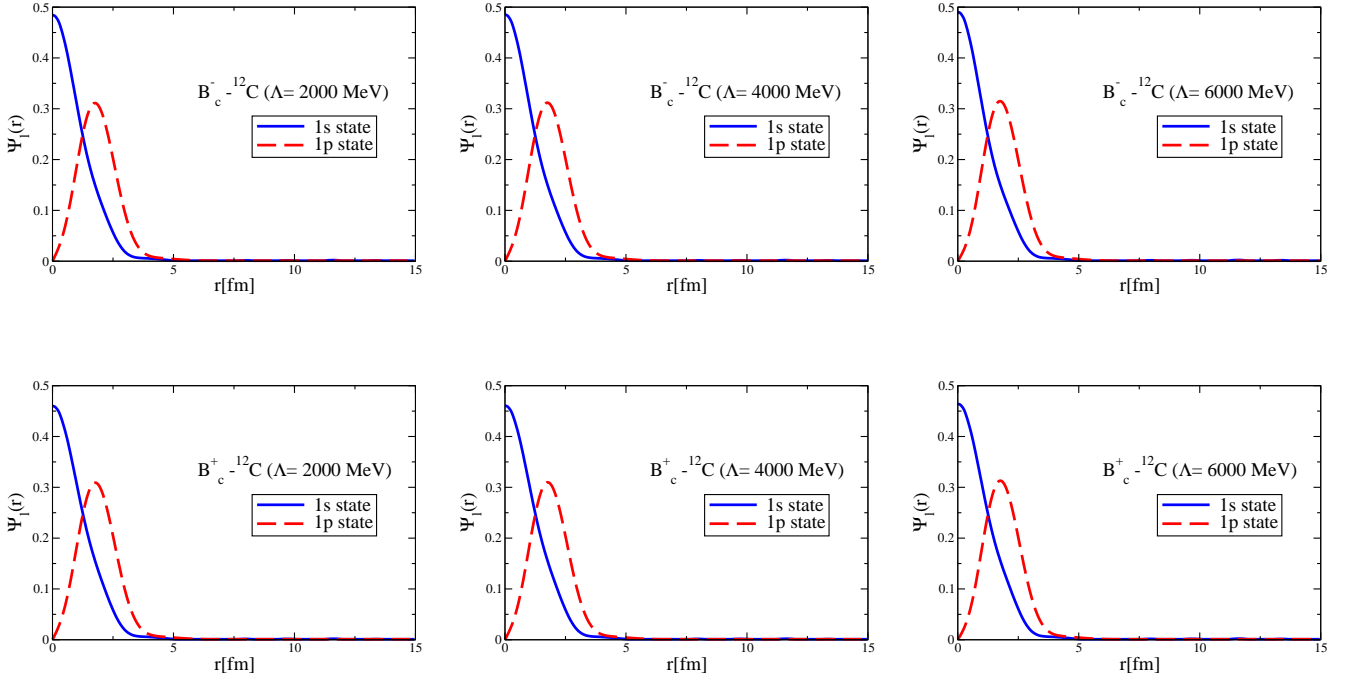


FIG. 28: Coordinate-space wave functions for the 1s and 1p states of the $B_c^\pm{}^{12}\text{C}$ systems with the Coulomb potentials for different values of Λ calculated using the direct Bessel transform.

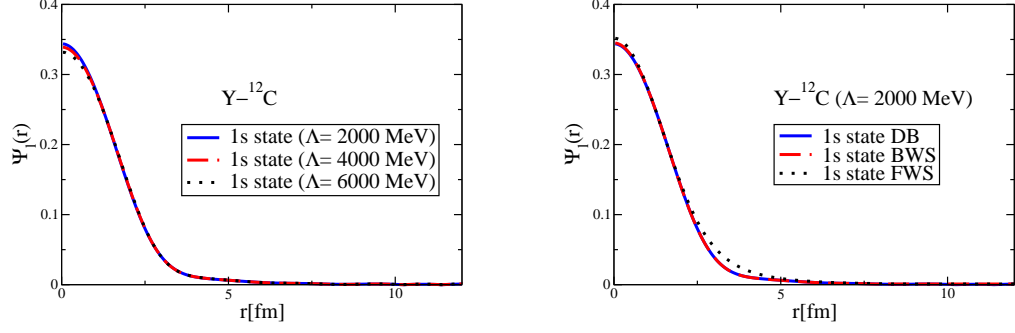


FIG. 29: 1s state wave functions of the Υ - ^{12}C system for different cutoff values (left) and momentum-space transformation methods (right).

TABLE X: The 1s ^{12}C bound state energies, obtained by the direct Bessel [Eq. (9)] and Woods-Saxon Fourier [Eqs. (A2) and (A3)] transform methods for $\Lambda = 2000$ MeV and different values of numerical error acceptance (indicated by "Error" in the Table) and number of integration points. (See Table VI for comparison.)

Bound state energies (GeV)		
Direct Bessel transform		
Error	NP = 100	NP = 200
10^{-5}	-0.013222572875961625	-0.013222565247691165
10^{-8}	-0.013222564819422189	-0.013222564814378224
10^{-16}	-0.013222564814095783	-0.013222564814095783
Woods-Saxon Fourier transform		
Error	NP = 100	NP = 200
10^{-5}	-0.010506281849386845	-0.010506341768125260
10^{-8}	-0.010506261966073183	-0.010506321862665757
10^{-16}	-0.010506261926916061	-0.010506321823470444